Gas Quantification Using Arrays of Intrinsic Zinc Oxide Thin Films Fabricated Using Three Different Successive Ionic Layer Adhesion and Reaction Processes

AMALLA, Bon Leif D.

April 16, 2019

Contents

List of Tables

List of Figures

Chapter 1

Introduction

1.1 Background of the Study

Zinc oxide is a metal oxide semiconductor that has many different uses based on its structure such as in thin film electronics. Zinc oxide thin films are used in a wide variety of applications as gas sensors (Florido & Dagaas, 2017) and as photovoltaic cells (Saikumar, Skaria, & Sundaram, 2014). In order for the material to perform predictably, it is necessary to be able to correlate processing parameters to structural characteristics and property manifestations (Florido & Dagaas, 2017; Saikumar et al., 2014).

Due to the promise of rapid, high-throughput materials processing brought by data science driven approaches to materials processing through materials knowledge systems (MKS) frameworks (Gupta, Cecen, Goyal, Singh, & Kalidindi, 2015; Sun, Cecen, Gibbs, Kalidindi, & Voorhees, 2017; Yabansu, Patel, & Kalidindi, 2014) the field of materials informatics has grown.

There are several studies on computational simulations regarding material properties based on material structure and vice versa (Gupta et al., 2015; Yabansu et al., 2014).

The MKS framework, as defined by Yabansu et al. (2014), is dependent on the definition of a microstructure function m_r^n, representing the probability density of finding a specific local

state $n \in N$, characterized by physical and chemical properties, at a spatial bin $r \in R$. A number of studies have proposed the MKS to use discretized microstructure functions in order to apply statistical measures (Gupta et al., 2015; Sun et al., 2017; Yabansu et al., 2014). Numerous studies regarding the use of MKS frameworks have produced different microstructure functions depending on the application of the materials of interest ranging from two to ten and more local states (Gupta et al., 2015; Sun et al., 2017; Yabansu et al., 2014).

Property homogenization, within a probe volume, can be easily achieved through calculation and regression of calculated two point spatial correlations derived from assumptions of periodicity of the microstructure function in a given probe volume V. Research done by Sun et al. (2017) has shown that the assumption of periodicity of the microstructure function in a probe volume can make drastic computational improvements to the MKS compared to using finite element methods.

Currently, there exists an implementation of the MKS framework in the Python programming language (PyMKS) (Wheeler, Brough, Fast, Kalidindi, & Reid, 2014). The said framework implementation is maintained by researchers Georgia Institute of Technology and has been developed by a number of contributors to the repository. It is currently available on Github as an open-source project licensed under the MIT license.

As a rapidly growing computational language, Julia has proven to be more efficient and effective as other computational programming languages such as Matlab, Python (NumPy), and Octave (Bezanson, Edelman, S., & Shah, 2015). Examples of scientific applications are as a simulator for different systems dynamics through BioSimulator.jl (Landeros et al., 2018), for different quantum systems through QuantumOptics.jl (Krämer, Plankensteiner, Ostermann, & Ritsch, 2018), and modeling protein electrostatics using finite element methods through NESSie.jl (Kemmer, Rjasanow, & Hildebrandt, 2018).

1.2 Objectives of the Study

The study aims to be able to define a new, simple microstructure function for the effective creation of MKS in developing material PSP linkages for the distribution of adhered particles of zinc oxide onto glass substrates. Specifically, the study will attempt to cover and discuss necessary measures that will aid in the creation of effective discrete spatial statistics of the particles, particle boundaries, and null spaces within the material structure, which will be used to find correlations to manipulations in the number of deposition cycles and annealing temperature.

The study also aims to be able to create a MKS methodology template in the Julia programming language. Specifically, the study aims to provide a new platform for materials informatics using the features of the programming language.

1.3 Significance of the Study

Some of the numerous applications of zinc oxide thin films are dependent on the different distribution-dependent properties of the material, including thin film sheet resistance, porosity, and transmittance. The computational modeling of zinc oxide material structure with respect to processing parameters and properties is a significant milestone for the rapid, high-throughput production of precise application-specific materials.

The expression of the MKS framework, case-dependent or independent, in multiple languages allows for the growth of the framework into several applications allowing open source communities to further develop the capabilities of the framework.

1.4 Scope and Limitations

The study mainly focuses on determining a family of microstructure functions that can be useful for building PSP linkages given sufficient material characterization. Since characterization is not readily accessible, structural characteristics used may be of low resolution. Thus, heavy caution must be observed in interpreting the results of the study.

Chapter 2

Review of Related Literature

2.1 Zinc oxide

2.1.1 Crystal structure

One of the key characteristics governing most of the properties of condensed matter is the crystal structure of a material. The crystal structure is thus important in characterizing material.

Zinc oxide is a metal oxide semiconductor having a hexagonal crystal structure. In studies such as those of Gao, Li, and Yu (2004) and Rajkumar et al. (2015), there are three identified main peaks in the diffaction pattern (see Characterization Methods) of zinc oxide. These three peaks are the first three peaks in the diffraction pattern of ZnO found roughly at $2\theta \in \{32^\circ, 34^\circ, 36^\circ\}$. The planes of diffraction are (100), (002), and (101), respectively, with the highest peaks at the (002) plane suggesting preferrential orientation in the c-axis. With regard to flat surfaces, this suggests formation of vertical rod-like structures from the substrates.

Numerous studies such as those of Gao et al. (2004), Vargas-Hernández, Jiménez-García, Jurado, and Henao Granada (2008a), and Rajkumar et al. (2015) have shown exper-

imentally that this structure of zinc oxide can be achieved even through production using different processes. All of these showed that manipulating the processing parameters have various effects on the crystalline structure of the material. They have effects on the crystallite size and relative intensities (diffraction). It is worth noting that the processes used for fabrication are SILAR processes, as will be described in a later section.

The three SILAR processes analyzed by Vargas-Hernández et al. (2008a) showed differences in the relative intensities of the diffraction peaks. It can also be noted that some of the diffraction peaks present in films fabricated by a process were not found in another. Rajkumar et al. (2015) showed how different doping concentrations affected the overall crystallinity of the thin film structure. The results, as expected, showed that different processing parameters lead to different material crystal structures.

2.1.2 Electrical properties

Studies have shown that zinc oxide thin films exhibit a wide variety of interesting properties such as *band gap* and *electrical resistivity*. Those of Rajkumar et al. (2015) and Vargas-Hernández et al. (2008a) made empirical studies on the effects of different processes on the electrical properties of ZnO. Specifically, Rajkumar et al. (2015) compared band gaps and electrical resistivity, while Vargas-Hernández et al. (2008a) compared band gap. Just as different processing parameters have led to differences in material crystal structures, the difference in crystal structures also reflect differences in material property.

Research on zinc oxide thin films as gas sensors by exploiting the reversible reactions of reducing gases to the surface of the material (Florido & Dagaas, 2017). These surface reactions change the movement of charges within the crystal structures of materials affecting their *resistivity*. There is more literature that shows how crystal structures affect the electrical resistivity and gas sensing response of metal oxide semiconductors from theoretical studies such as of Dey (2018) and Hua et al. (2018) to *in silica* studies like involving DFT (Zhao et al.,

2013); however, these will not be focused on in this study.

The importance of being able to computationally predict the properties similar to the *in silica* study referred to above is a huge milestone in predicting properties given the structure of a material.

2.1.3 Successive ionic layer adhesion and reaction processes

Successive ionic layer adhesion and reaction (SILAR) processes are a family of processes wherein materials are deposited onto substrates by means of successive surface reactions. The processes described will be based on the study by Gao et al. (2004).

The processes consist of two main phases: a *deposition* phase and an *annealing* phase. The deposition phase in material fabrication involves a set of precursor solutions: cationic solutions, complexing solutions, and anionic solutions, to perform the reactions on the surface of the substrate. The three solutions are aqueous (Gao et al., 2004). Thus, the substrate surface must be hydrophilic for the solutions to react in the and adhere. However, naturally, glass is hydrophobic which can be noted by the formation of droplets on its surface. Gao et al. (2004) suggested the following methodology to develop the hydrophilic property of glass surface: boil the substrates in dilute H_2SO_4 (1 : 10 v/v) for 30 minutes, then completely rinse the substrates in ethanol, acetone, and de-ionized water. Similar processes were also done by Rajkumar et al. (2015) and Vargas-Hernández et al. (2008a).

A study conducted by Vargas-Hernández, Jiménez-García, Jurado, and Henao Granada (2008b) was performed in order to determine the effects of three different number of deposition cycles to thin film crystallinity. It was observed that the relative intensities of the diffraction peaks drastically increased with the number of deposition cycles. However, there was no literature, as of this manuscript, that can be used to explain this phenomenon. It should be noted that the studies conducted by Vargas-Hernández et al. (2008b) and Vargas-Hernández et al. (2008a) differ in the parameter tested in SILAR processing.

In addition to the precursor solutions and substrate properties described, another factor that affects the output of SILAR processes is the drying interval being deployed between each dipping processes (Gao et al., 2004). In the cited literature, the researchers compared the effects of two drying processes in the crystallinity of the thin films. In applying a drying process of $3-5$ or 30 seconds between each deposition *cycle*, the resulting thin films have a defined and *periodic* microstructure. Those films processed with no drying process between each deposition cycle were found to have *amorphous* microstructures.

The annealing process in SILAR processes is crucial for the growth of crystal structures in the thin film. According to Rajkumar et al. (2015), it is still unknown how, specifically, annealing affects this growth. There are numerous *empirical* studies regarding this topic, however, there is currently no solid theory known to the researchers as of date.

In the study of Rajkumar et al. (2015), it can be observed through the XRD spectra that annealing plays a huge role in the development of crystal structures. It can be seen that the measured intensities at the Bragg angles stated above have increased. This means that better crystallinity is achieved through thermal annealing. The study of Gao et al. (2004) has found that there can also be different effects on thin film crystallinity based on the annealing environment used. It can be inferred from the data that the adjusting the annealing environment leads to different average crystallite sizes within the thin films.

Studies by Vargas-Hernández et al. (2008a), Vargas-Hernández et al. (2008b), Gao et al. (2004), and Rajkumar et al. (2015) all have used different precursor solutions in preparing thin films.

2.2 Multiscale Modeling

2.2.1 Representative volume elements

Crucial in most multiscale modeling methodologies is the development of elements of finite volume that reflects the general physics of the macrostructure. Representative volume elements (RVE) are images of the material chosen such that the overall distribution of the *local states* and their interactions may be able to represent the underlying mechanisms (physics) of the whole structure at a particular length scale. From here onward, the terms regarding RVEs will be defined as follows:

1. Probe volume (S) - *material volume* being studied (same as RVE)
2. Voxel (s) - *small, discrete* volume elements taken from an RVE ($s \in S$)
3. Local state space (H) - set of all realizable physical and chemical properties representing material characteristics at a *particular length scale*
4. Local state (h) - an element of the local state space ($h \in H$)
5. Boundary conditions ($\aleph$) - a set of requirements for interactions within S

These definitions are important in establishing concepts regarding the use of RVEs in different property homogenization models. As will be seen in later discussions, S and $\aleph$, but not s, H, h, will have slightly varied definitions depending on the data needed by specific modeling techniques.

2.2.2 Finite element methods

Finite element methods rely on computer simulations of mechanical theories on finite, discrete elements $s \in S$. This means that this method can be used to simulate and study the effects of mechanical systems with respect to space and their interactions with one another. An

interesting study done by Carniel, Khlar, and Fancello (2019) dealt with finding an optimal ℵ, with regard to the case, conditions to be met incorporating the interaction of collagen fibers ($h_1 \in H$) and the surrounding cellular matrix ($h_2 \in H$). In finite element considerations, however, these are not the only conditions that must be followed. Energy conformation conditions also have to be observed (Li, Liu, & Zhang, 2010).

The work of Li et al. (2010) dealt with the establishment of a mathematical derivation of a model for microstate property homogenization. Their work, split into six sections of rigorous mathematical manipulation, involves these steps: expression of Cauchy continuum energy and mechanical conformation conditions into Cosserat continuum conditions, the development of a homogenization model, and establishment of ℵ. The steps in proof done by these researchers present a method in developing homogenization models using different representations of an RVE. It is worth noting that the definition of the RVE is flexible for as long as proper conditions are imposed.

These finite element methods are *very* effective in modeling the interactions of different materials and their configurations within an RVE. Due to the complexity of the implementation of this method, computer simulations may run for hours, which is not efficient in rapid, high-throughput materials processing.

2.2.3 Deep learning methods

With the development of the various fields of artificial intelligence, many different modeling techniques have been developed, especially in the areas of image recognition, and multivariable property prediction with the use of convolutional and artifical neural networks. A homogenization model was developed by Kondo, Yamakawa, Masuoka, Tajima, and Asahi (2017) for predicting the ionic conductivity of ceramics using convolutional neural networks. The research was done in order to determine the feasibility of using convolutional neural networks in microstructure image processing, and to predict the desired property from image

analyses.

The RVEs used by the CNN are *raw* images of the material at particular length scales. The researchers aimed to determine how the length scale of the RVE affected the accuracy of their model. Note that the computer images are analyzed through discrete elements s as image pixels. The study used a completely different representation of RVEs from those used by finite element studies such as of Carniel et al. (2019) and Li et al. (2010). In the study it has been found that it is possible to perform image analysis on a small number of RVEs with a definite size (enough to distinguish between different h). The researchers were able to only use seven images in the prediction of the property of interest with "acceptable" accuracy.

One of the problems with using advanced artificial intelligence methodologies, as admitted by Kondo et al. (2017), was the uninterpretability of the model. In order to circumvent this problem and to provide a basis for model classification and prediction, the researchers have provided "saliency maps" to see how the CNN classified the local states and inferred the interaction of such local states through implicit $\aleph$. This may be a good protocol on studying how CNNs work internally and provide a one-way theories to predict desired properties.

Another problem posed by the use of CNNs, not mentioned in the research, is the unidirectional flow of information. As evident from the research, the desired property, given different RVEs can be calculated; however, even with the introduction of saliency maps, it may still be difficult to reconstruct an RVE and its processing history from the properties desired. This is the case with most engineering problems.

2.3 Materials knowledge systems

2.3.1 Microstructure functions

The materials knowledge framework is a data science framework developed for the relatively simple modeling of material process, structure, and property. This framework will

be the modeling methodology of interest of the study. A careful review of the data analysis framework will be given as follows.

The materials knowledge systems (MKS) framework rests upon the definition of microstructure functions. This probability density function ($m(\vec{x},h)$) has the following properties (Niezgoda, Fullwood, & Kalidindi, 2005):

$$m(\vec{x},h)dH = \frac{^hV}{V}\bigg|_{\vec{x}}$$

This means that the probability density of finding a local state $dH = h$ can be expressed as the volume fraction of the h within $V = dS$. By summing over the local state space H, the probability should add up to 1 by definition of the local state space.

$$\int_H m(\vec{x},h)dH = 1$$

From these descriptions, analogous expressions can be defined for discrete data.

$$\sum_S {}^h m_s = {}^h V|S| \qquad\qquad \sum_{h=1}^{H} {}^h m_s = 1$$

The probability function ${}^h m_s$ gives the volume fraction occupied (the expected probability) of the local state defined by h in the voxel s.

With the definition of discrete microstructure functions, it is possible *for computers* to perform calculations from various data relating to RVEs. Operations on probabilities and images may be applied. Examples of these operations include calculation of spatial statisitics (N-point spatial correlations), which have been used in quite a number of studies. In each of these studies, there appears to be a different method for defining h_i, and hence H, depending on the properties being studied in materials.

Studies conducted by Yabansu et al. (2014), Niezgoda et al. (2005), de Oca Zapain, Popova, and Kalidindi (2017), and Sun et al. (2017) have used different methods in defining

the local state space H depending on which definition will yield more *computationally efficient* results. The ones cited are studies on two-phase material systems, polycrystalline systems, and other composite material systems.

Sun et al. (2017) studied dendritic structures in a *two-phase* non-parallelepiped RVEs. They have shown through a case study that it is possible to apply different image processing techniques such as image masking and padding for the calculation of spatial correlations from modified microstructure functions. They have done this through the introduction of padding modifications and masking functions, which directly change the algorithm for the calculation of spatial correlations. In this two-phased material structure, given that image resolution is fine enough, states h_0 and h_1, *eigenstates*, are assigned to the voxels $s \in S$. These eigenstates are defined as follows:

$$h_0 = 0 \qquad\qquad h_1 = 1$$

The use of h_1 for the identification of a local state h indicates that h_1 occupies the entirety of s, while h_0 is used for representing the other local state. One problem as noted of this classification is the fact that the definition of H may be based on researcher bias (Kondo et al., 2017).

Yabansu et al. (2014) and de Oca Zapain et al. (2017) did studies on the possible prediction of properties in polycrystalline material systems with the use of the MKS framework. Since both studies have noticed the tremendous amount of local state representation using Euler-Bunge angles, they have decided to use generalized spherical harmonics to define H. With these efforts, the computations were drastically reduced! The method used will not be discussed in detail for it is outside the scope and applications of the study.

Niezgoda et al. (2005) worked on the delineation of the properties of spatial correlations in multiphase composite systems. They have introduced the concept of *hulls* such as one-point and two-point spatial correlation hulls that define the physically realizable spatial correlations

given the training dataset.

Discrete microstructure functions ${}^{h}m_s$ explain *only* the probability density of finding local states h at small voxels s (Cecen, Yabansu, & Kalidindi, 2018). They have also remarked that the measure is not *translation-invariant*, *i.e., assumptions in statistics are not directly applicable*. This can be circumvented by the definition of *N-point statistics* such as one-point and two-point spatial correlations as will be discussed for the next subsections.

2.3.2 One-point spatial correlations

One-point spatial correlations define the expected probability of the local state to appear in the whole RVE. This is equivalent to the *volume fraction* occupied by a certain h for in S. By rearrangement of an equation above:

$$f(h) = \frac{1}{|S|} \sum_{S} {}^{h}m_s = {}^{h}V$$

Using the microstructure functions themselves, the one-point statistic for a discrete distinguishable h is the *volume average* of the probability. The calculation of the this statistic is easy and increases linearly with respect to the size of the RVE.

2.3.3 Two-point spatial correlations

Two-point correlations are a type of N-point statistics that define the *joint probability* of locating two local states within voxels s separated by a displacement vector $\vec{t}$. Usually, to define these statistics and easily evaluate them, the vectors are assigned into indices from 0 to $|S-1|$. The "translation-invariant" two-point spatial correlations are defined as:

$$f(hh'|t) = \frac{1}{|S|} \sum_{t \in S} {}^{h}m_s \, .^{h'} \, m_{s+t}$$

The studies mentioned above, including Cecen et al. (2018), have different methods

of calculating two-point spatial correlations because of the difference in definition of the microstructure function.

Calculation of values

All of the cited literature on the topic similarly defined two-point spatial correlations as a *convolution* operation on two probability densities. They all have exploited the transformation of the microstructure function into spectral space via discrete Fourier transforms (DFT). The properties of complex numbers have been exploited in many different ways by the cited literature in calculating the said statistics.

The calculations in spectral space have been shown to have drastically reduced time complexities (Niezgoda et al., 2005). Cecen et al. (2018) used the expression of complex numbers in polar form to describe "rotationally invariant" spatial correlations in spectral space. The use of mask functions and padding operations (Sun et al., 2017) redefined the calculations of two-point statistics in non-parallelepiped material systems. The use of Bunge-Euler angles in the reduction of local states (de Oca Zapain et al., 2017; Yabansu et al., 2014) were helpful in reducing the amount of calculations needed.

Chapter 3

Methodology

3.1 Thin Film Fabrication

Thirty glass substrates, measuring 1" $\times$ 0.25", were cut from microscope slides. These substrates were subject to three successive ionic layer adhesion and reaction (SILAR) processes, S1, S2, and S3, as will be detailed in this section. All of the SILAR processes consist of a certain number of deposition cycles from a fixed precursor solution with $0.095M$ Zn^{2+} and $0.190M$ NaOH and a thermal annealing at certain temperatures (Florido & Dagaas, 2017; Gao et al., 2004).

Table 3.1 summarizes the different SILAR processes along with the variations in processing parameters.

Table 3.1: Processing parameters manipulated and SILAR processes

—	S1	S2	S3
Depostion cycles	100	75	100
Annealing temperature	450°C	450°C	500°C

1	3
2	4

Figure 3.1: Basic orientation matrix

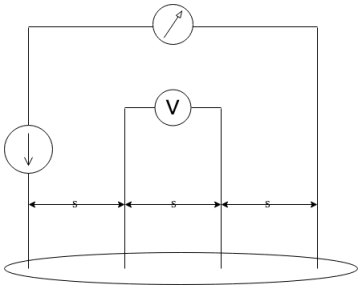

Figure 3.2: Four point probe mechanism for determination of sheet resistance

3.2 Thin Film Characterization

The fabricated thin films were characterized for determination of thin film structure and properties.

One thin film fabricated using each of the fabrication processes was chosen for optical microscopy. The fabricated material was split into four sections as shown in Figure 3.1. The sections were chosen such that the four corners of the rectangular substrate represent different probe volumes. The thin films were viewed under the high power objective lens ($400\times$) of a digital compound microscope.

Overall thin film structure were also characterized with x-ray diffraction, using Cu-Kα anode ($\lambda = 1.54\,\text{Å}$), and scanning electron microscopy at $20\,\text{kV}$.

Finally, the thin films sheet resistance values were derived from measurements from four-point probe sensing. The schematic for the four-point probe mechanism are shown in Figure 3.2.

3.3 Model Creation

3.3.1 Definition of microstructure functions

There are a total of 20 discrete microstructure functions (DMF) that are studied for the study. The definitions are divided into four categories depending on which of two axes will the DMFs be assumed to be periodic in. Each of the four categories contains five DMFs, which differ based on the method for determining the number of discrete local states within a certain probe volume V.

The functions can be summarized as Table 3.2. The dimensions of the probe volume V were chosen as odd products of small primes (2, 3, 5, and 7) to aid in the computation of two point spatial correlations, as will be discussed in the following subsection, with the exception of one function, with accounts for the dimensions of the size of a high resolution digital image.

3.3.2 Calculation of two-point spatial correlations

Two point spatial correlations are derived from optical microscopy images through the definition of the measures (Gupta et al., 2015).

$$m_r^{np} = \frac{1}{S_r N} \sum_{i=0}^{N} \sum_{i=0}^{R} m_r^p m_r^n$$

where n, p are the discrete local states of interest and r is the spatial bin of interest.

Image data were transformed into Julia 2D arrays (Bezanson et al., 2015) and further into a user defined data structure named *MaterialImage* which accounts for the parameters used for defining the DMFs (from the previous subsection). There are a total of 20 sets two point spatial correlations that will be considered.

Table 3.2: Summary of discrete microstructure functions

Periodic axes	Local states	Size of V
Both i, j	Two	225×225
Both i, j	Two	441×441
Both i, j	Three	225×225
Both i, j	Three	441×441
Both i, j	Three	1920×1080
j	Two	225×225
j	Two	441×441
j	Three	225×225
j	Three	441×441
j	Three	1920×1080
i	Two	225×225
i	Two	441×441
i	Three	225×225
i	Three	441×441
i	Three	1920×1080
None	Two	225×225
None	Two	441×441
None	Three	225×225
None	Three	441×441
None	Three	1920×1080

3.3.3 Determination of optimal film orientation

Since the preferred orientation of the fabrication of thin films is unknown, each of the three thin films have four hypothesized orientations based on circular permuations of the orientation matrix (Figure 3.1).

For each of the calculated two point spatial correlations, the values will undergo principal component analysis to obtain the orthogonal latent descriptors (Gupta et al., 2015; Sun et al., 2017). This is done with *MultivariateStats.jl*, a package available for multivariate statistical analysis (Dahua, 2018). Optimal orientation is determined when the variance of the dimensionally-reduced two point statistics, *i.e. the matrix trace of the covariance matrix* is minimized.

3.3.4 Determination of optimal microstructure function

The plots for the two-point statistics are manually compared. Partial least squares analysis (PLSA) is done to compare the ability of the DMF to capture the variation of derived sheet resistance values. Evaluation of the optimal microstructure function will be based on the following parameters:

1. Variance capture via PLSA

2. Qualitative assessment of clustering of microstructure ensembles

Chapter 4

Results and Discussion

4.1 Thin film characterization

4.1.1 Images from optical microscopy

Figure 4.1 shows images of thin films under a 40× magnification. From the images it can be observed that material does not completely cover the whole substrate. Moreover, the distribution of the particles was random, as was verified by image analysis techniques from the MKS framework in a later discussion.

This means that **no** accurate measurements about the specific properties of the material can be measured in the length scale. In order to measure the resistivity of the material, for example, it is important that the material completely covers the length from the current source

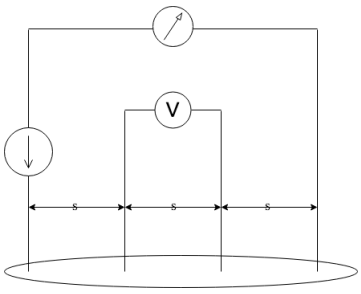

Figure 4.1: Material images taken under high power objective lens of compound microscope.

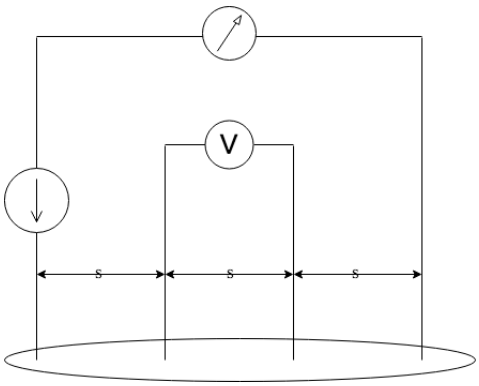

Figure 4.2: Material images taken under scanning electron microscope at different magnification values. The images show the crystals present, particle distribution, and film thickness.

and sink for four-point probe sensing. Since there are spaces between material structures, electrical resistance is increased by the interaction with glass. It can be said that the formation of material using the processes specified were not able to yield replicable results.

4.1.2 Images from scanning electron microscopy

Figure 4.2 shows images of thin films under a multiple magnification levels. One of the images show the side profile of one of the thin films showing its thickness. The thickness of the film is reported to be 50 µm. Comparing to Florido and Dagaas (2017), the thickness of the fabricated thin film was reported to be 50 µm. This indicates that the processes used produced films of similar thickness despite the difference in number of deposition cycles used.

4.1.3 Energy dispersive spectroscopy analysis

Figure 4.3 shows the EDX spectra showing the different atoms present in a part of the sample.

4.1.4 Structure elucidation from x-ray diffraction

Figure 4.4 shows the x-ray diffraction spectra of the thin films.

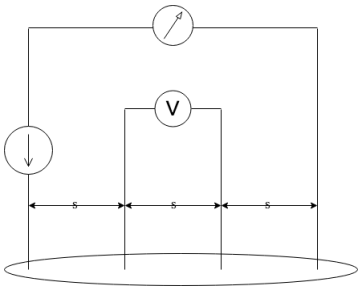

Figure 4.3: Energy dispersive spectroscopy spectra of sections in thin film samples.

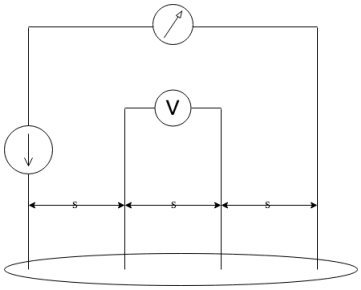

Figure 4.4: X-ray diffraction spectra of thin film samples

4.1.5 Four-point probe sensing

Table 4.1.5 shows the average sheet resistance values along with the statistical range.

4.2 Development of materials knowledge framework

4.2.1 Calculation of two point spatial correlations

Two point spatial correlations (autocorrelations) were calculated based on two main material phases as seen in the optical microscopy images: the presence and absence of zinc oxide in the structure. Contour plots showing the statistics are shown in Figure 4.5.

1	2	3
4	5	6

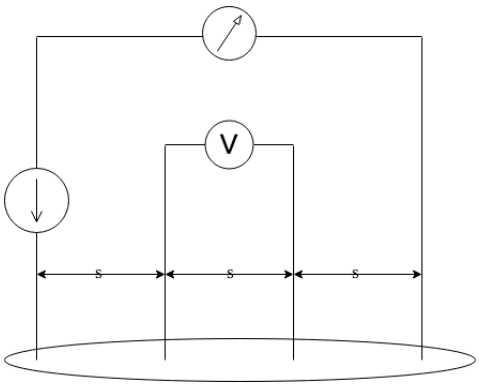

Figure 4.5: Contour plots showing autocorrelations of the probability of finding zinc oxide in the material. It can be analytically shown that the autocorrelation for the absence of zinc oxide is similar in distribution.

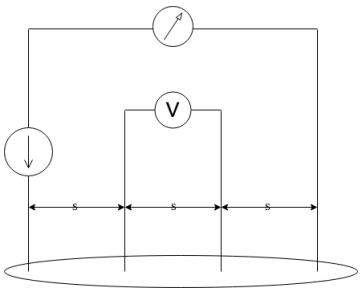

Figure 4.6: Dimensionally-reduced spatial correlations

4.2.2 Principal component analysis and DMF comparison

The autocorrelations underwent principal component analysis for dimensional reduction. This was used to determine whether there are significant difference to the autocorrelations within the structures and to determine of there are processing factors affecting the difference. Some of the plots are shown as Figure 4.6.

4.2.3 Partial least squares analysis

Unfortunately, due to the homogeneity of the samples as shown by the two point spatial correlations, no partial least squares model can be made from the data to capture the difference in sheet resistance.

Chapter 5

Summary and Conclusions

Zinc oxide thin films were fabricated using three different successive ionic layer adhesion and reaction processes. The material structure was partially elucidated using characterization techniques such as optical microscopy, scanning electron microscopy, energy dispersive spectroscopy, and x-ray diffraction. It was found out that the particle distribution among the three processes are random and do not exhibit significant differences. From here, no stable relationships can be made between material phase distribution. It was concluded that the difference in thin film property was due to the difference in crystal structure. The project was unsuccessful in comparing the material state autocorrelations and material property.

Chapter 6

Recommendations

It is recommended to study the effects of the crystal structures and orientations on the electrical properties of the fabricated material. This means that there should be more than two material phases to be considered and studied using the MKS framework application. This is because of the random and homogeneous distribution of crystalline material in the substrate. Other thin film fabrication processes may be considered and studied.

References

Bezanson, J., Edelman, A., S., K., & Shah, V. B. (2015). Julia: A fresh approach to numerical computing. *Society for Industrial and Applied Mathematics*, *59*, 65–98.

Carniel, T. A., Khlar, B., & Fancello, E. A. (2019). On multiscale boundary conditions in the computational homogenization of an RVE of tendon fascicles. *Journal of the Mechanical Behavior of Biomedical Materials*, *91*, 131–138.

Cecen, A., Yabansu, Y. C., & Kalidindi, S. R. (2018). A new framework for rotationally invariant two-point spatial correlations in microstructure datasets. *Acta Materialia*, *158*, 53–64.

Dahua, L. (2018). Multivariatestats documentation [Computer software manual]. Retrieved 24 Jan 2018, from `media.readthedocs.org/pdf/multivariatestatsjl/latest/multivariatestatsjl.pdf`

de Oca Zapain, D. M., Popova, E., & Kalidindi, S. R. (2017). Prediction of microscale plastic strain rate fields in two-phase composites subject to an arbitrary macroscale strain rate using the materials knowledge system framework. *Acta Materialia*, *141*, 230–240.

Dey, A. (2018). Semiconductor metal oxide gas sensors: A review. *Materials Science and Engineering B*, *229*, 206–217.

Florido, E. A., & Dagaas, N. A. C. (2017). Carbon monoxide gas sensing using zinc oxide deposited by successive ionic layer adhesion and reaction. *IOP Conf. Series: Materials Science and Engineering*, *201*.

Gao, X. D., Li, X. M., & Yu, W. D. (2004). Synthesis and optical properties of ZnO nanocluster porous films deposited by modified SILAR method. *Applied Surface Science*, *229*, 275–281.

Gupta, A., Cecen, A., Goyal, S., Singh, A. K., & Kalidindi, S. R. (2015). Structure-property linkages using a data science approach: Application to a non-metallic inclusion/steel composite system. *Acta Materialia*, *91*, 239–254.

Hua, Z., Tian, C., Huang, D., Yuan, W., Zhang, C., Tian, X., ... Li, E. (2018). Power-law response of metal oxide semiconductor gas sensors to oxygen in presence of reducing gases. *Sensors and Actuators B: Chemical*, *267*, 510–518.

Kemmer, T., Rjasanow, S., & Hildebrandt, A. (2018). NESSie.jl: Efficient and intuitive finite element and boundary element methods for nonlocal protein electrostatics in the Julia language. *Journal of Computational Science*, *28*, 193–203.

Kondo, R., Yamakawa, S., Masuoka, Y., Tajima, S., & Asahi, R. (2017). Microstructure recogntion using convolutional neural networks for prediction of ionic conductivity in ceramics. *Acta Materialia*, *41*, 29–38.

Krämer, S., Plankensteiner, D., Ostermann, L., & Ritsch, H. (2018). QuantumOptics.jl: A Julia framework for simulating open quantum systems. *Computer Physics Communications*, *227*, 109–116.

Landeros, A., Stutz, T., Keys, K. L., Alekseyenko, A., Sinsheimer, J. S., Lange, K., & Sehl, M. E. (2018). Biosimulator.jl: Stochastic simulation in Julia. *Computer Programs and Methods in Biomedicine*, *167*, 23–35.

Li, X., Liu, Q., & Zhang, J. (2010). A micro-macro homogenization approach for discrete particle assembly: Cosserat continuum modeling of granular materials. *International Journal of Solids and Structures*, *47*, 291–303.

Niezgoda, S. R., Fullwood, D. T., & Kalidindi, S. R. (2005). Delineation of the space of 2-point correlations in a composite material system. *Acta Materialia*, *56*, 5285-5292.

Rajkumar, P. V., Ravinandran, K., M., B., Ravidhas, C., B., S., & Dineshbabu, N. (2015). Enhancement of optical and electrical properties of SILAR deposited ZnO thin films through fluorine doping and vacuum annealing for photovoltaic applications. *Materials Science in Semiconductor Processing*, *35*, 189–196.

Saikumar, A. K., Skaria, G., & Sundaram, K. B. (2014). ZnO gate based MOSFETs for sensor applications. *ECS Transactions*, *61*, 65–69.

Sun, Y., Cecen, A., Gibbs, J. W., Kalidindi, S. R., & Voorhees, P. W. (2017). Analytics on large microstructure datasets using two-point spatial correlations: Coarsening of dendritic structures. *Acta Materialia*, *132*, 374–388.

Vargas-Hernández, C., Jiménez-García, F. N., Jurado, J. F., & Henao Granada, V. (2008a). Comparison of ZnO thin films deposited by three different SILAR processes. *Microelectronics Journal*, *39*, 1349–1350.

Vargas-Hernández, C., Jiménez-García, F. N., Jurado, J. F., & Henao Granada, V. (2008b). XRD, μ-Raman and optical absorption investigations of ZnO deposited by SILAR method. *Microelectronics Journal*, *39*, 1347–1348.

Wheeler, D., Brough, D., Fast, T., Kalidindi, S., & Reid, A. (2014). *Pymks: Materials knowledge system in Python.*

Yabansu, Y. C., Patel, D. K., & Kalidindi, S. R. (2014). Calibrated localization relationships for elastic response of polycrystalline aggregates. *Acta Materialia*, *81*, 151–160.

Zhao, L., Tian, F., Wang, X., Zhao, W., Fu, A., Shen, Y., ... Yu, S. (2013). Mechanism of CO absorption on hexagonal WO_3 (001) surface for gas sensing: A DFT study. *Computational Materials Science*, *79*, 691–697.